

Selective amplification of the chirped attosecond pulses produced from relativistic electron mirrors

Letter to the Editor

Cite this article: Tan F *et al.* (2020). Selective amplification of the chirped attosecond pulses produced from relativistic electron mirrors. *Laser and Particle Beams* **38**, 165–168. <https://doi.org/10.1017/S0263034620000142>

Received: 22 January 2020


Accepted: 8 April 2020

Key words:

Laser-driven electron acceleration; particle-in-cell method; relativistic electron mirror

Author for correspondence:

Y. Q. Gu, Laser Fusion Research Center, China Academy of Engineering Physics, Mianyang, China. E-mail: yqgu@caep.cn

F. Tan^{1,2} , S. Y. Wang², B. Zhang², Z. M. Zhang², B. Zhu², Y. C. Wu², M. H. Yu², Y. Yang², G. Li², T. K. Zhang², Y. H. Yan², F. Lu², W. Fan², W. M. Zhou² and Y. Q. Gu²

¹Department of Modern Physics, University of Science and Technology of China, Hefei 230026, China and

²Laser Fusion Research Center, China Academy of Engineering Physics, Mianyang, China

Abstract

In this paper, the generation of relativistic electron mirrors (REM) and the reflection of an ultra-short laser off the mirrors are discussed, applying two-dimension particle-in-cell simulations. REMs with ultra-high acceleration and expanding velocity can be produced from a solid nanofoil illuminated normally by an ultra-intense femtosecond laser pulse with a sharp rising edge. Chirped attosecond pulse can be produced through the reflection of a counter-propagating probe laser off the accelerating REM. In the electron moving frame, the plasma frequency of the REM keeps decreasing due to its rapid expansion. The laser frequency, on the contrary, keeps increasing due to the acceleration of REM and the relativistic Doppler shift from the lab frame to the electron moving frame. Within an ultra-short time interval, the two frequencies will be equal in the electron moving frame, which leads to the resonance between laser and REM. The reflected radiation near this interval and corresponding spectra will be amplified due to the resonance. Through adjusting the arriving time of the probe laser, a certain part of the reflected field could be selectively amplified or depressed, leading to the selective adjustment of the corresponding spectra.

Introduction

Ultra-short X-ray is a powerful tool for detecting the atom and molecule motions within the femtosecond time scale (Attwood, 1999). Among many methods of generating X-ray pulses, Thomson scattering source is a promising way to produce quasi-monoenergetic and energy tunable X-ray pulses with femtosecond duration and high brightness (Sprangle and Esarey, 1992; Sprangle *et al.*, 1992). But the tiny cross section of the Thomson scattering and the low photon yield restrict the practical applications. To increase the photon yield, the high-density electron layer produced by laser-plasma interaction is suggested as a relativistic electron mirror (REM) to reflect another laser beam (Bulanov *et al.*, 2003), where the high electron density will lead to much higher photon yield. This method opens a possible way to generate ultra-high-intense electromagnetic fields towards the Schwinger Limit.

The numerical studies on the interaction between ultra-high-contrast laser and solid nano-film targets show the possibility to directly push a whole electron layer from the targets (Kulagin *et al.*, 2007). The REM radiation studies have attracted many theoretical (Habs *et al.*, 2008; Esirkepov *et al.*, 2009; Meyer-ter-Vehn and Wu, 2009; Wen *et al.*, 2009; Wu and Meyer-ter-Vehn, 2009; Wu *et al.*, 2010, 2011; Wu, 2011; Tan *et al.*, 2012; Wen *et al.*, 2012) and experimental efforts (Kiefer *et al.*, 2009, 2013). In recent review papers (Bulanov *et al.*, 2013, 2016), the mechanism of generating the REM and frequency upshifted radiation pulse has been presented. Although the reflectivity of relativistic ultra-thin electron layers can be analytically derived (Wu and Meyer-ter-Vehn, 2009; Bulanov *et al.*, 2016), the reflectivity under the resonance condition, when the plasma frequency of the REM is equal to the laser frequency, cannot be well described.

In this paper, the simulation results for the generation of REM and the reflection of an ultra-short probe laser off the REM are introduced. Rapidly accelerating and expanding REM can be generated from a nanofoil target illuminated normally by an ultra-intense femtosecond laser pulse. Isolated chirped radiation pulse can be produced from the reflection of a counter-propagating probe laser on the REM. In the reflected radiation field, an unusual intense peak is observed. Considering this peak is produced by the frontier of the probe laser with lower intensity, we can say that the reflected radiation is amplified around this peak. Through analyzing the plasma frequency of the REM and the frequency of the probe laser in the electron moving frame, it is found that the two frequencies will be equal at the moment right before the amplification of the reflected radiation occurs. So this amplification can be attributed to the resonance between plasma oscillation in the REM and the probe laser in

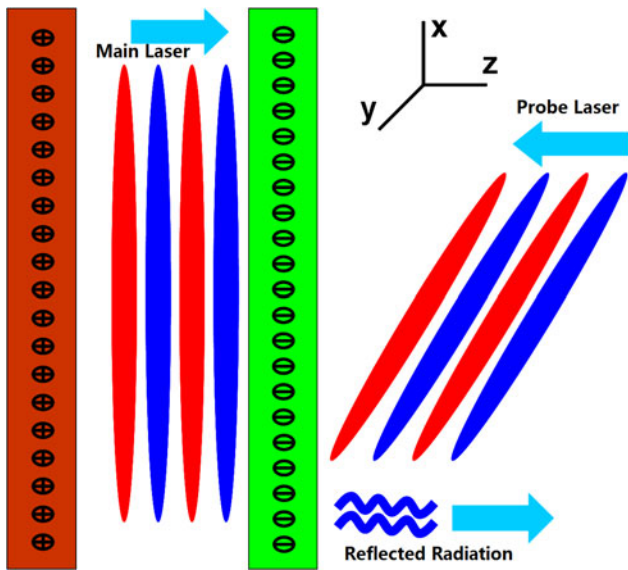


Fig. 1. Schematic drawing of the interaction process in our PIC simulations.

the electron moving frame. Based on this phenomenon, the arriving time of the probe laser can be adjusted in order to selectively amplify or depress the reflected field from REM, leading to the selective adjustment of the corresponding spectra.

Simulation parameters

To study the generation of the REM and the reflection of the probe laser by the REM, we performed two-dimensional particle-in-cell (2D PIC) simulations using the Vorpil code (Nieter and Cary, 2004). The schematic drawing of the interaction process is shown in Figure 1. An ultra-intense femtosecond laser pulse normally illuminates on a nanofoil. The electrons in the target are pushed out as a whole electron layer, which forms a REM. During the acceleration of the electron layer, a second probe laser pulse irradiating normally on the layer can be reflected, producing an isolated radiation pulse. The simulation box has a size of $10\lambda \times 20\lambda$ in the zx plane, and spatial resolution of $1000 \text{ cells}/\lambda$ both in the z and x direction. The main laser is linearly polarized along x axis and propagates from the left boundary of the simulation box to right. This pulse has a profile of $a_0 \sin^2(\pi t/T)$ with pulse duration $T = 4\lambda/c$ and wavelength $\lambda = 800 \text{ nm}$. The transverse intensity profile is $\exp(-r^2/R^2)$, where $R = 5\lambda$ is the transverse half width at $1/e^2$ of maximum intensity. The normalized laser field a_0 is 100. The counter-propagating probe laser is linearly polarized along y axis and propagates from the right boundary of the simulation box to left. The parameters of the counter-propagating probe laser are all the same with the main laser except for the smaller normalized laser field $a_0 = 0.1$. The smaller intensity can make sure that the REM would not be disturbed distinctly by the probe laser. An ultra-thin nanofoil is used as the target placed perpendicular to the main laser direction. The foil is located at $z_1 = 5\lambda = 4 \mu\text{m}$ with a thickness of $d = 2.4 \text{ nm}$. The electron density of the target is $n_e = 1.315 \times 10^{29} \text{ m}^{-3}$, corresponding to $75 n_c$. n_c is the critical density for laser wavelength of 800 nm .

Simulation results and analysis

At two chosen moments 14.7 and 15.4 fs, the spatial distribution of REM and the corresponding radiation field at the same time

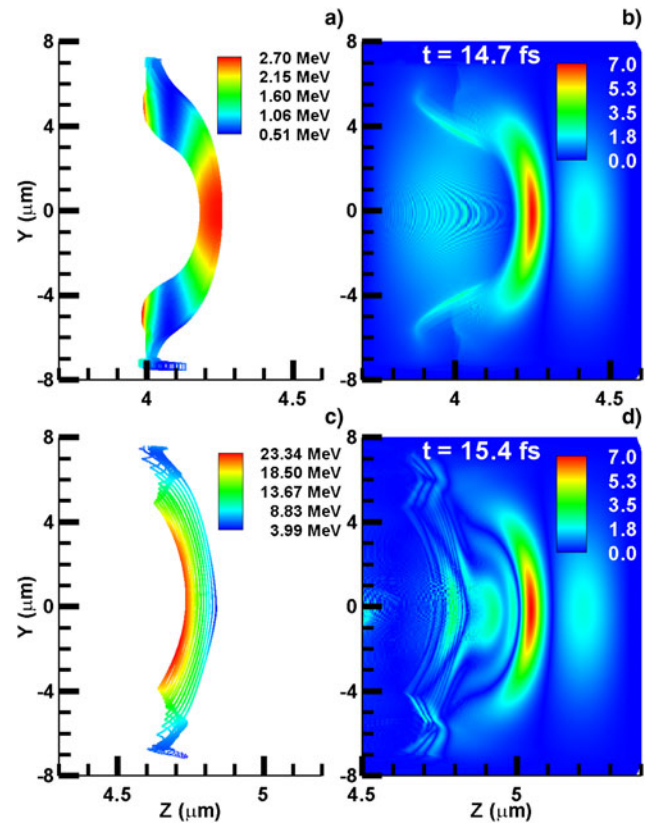


Fig. 2. The spatial distribution for (a), (c) the electron layer and (b), (d) the generated radiation field at the same time. The first and second row correspond to the results at 14.7 and 15.4 fs, respectively. The unit of the radiation field is 10^{10} V/m .

are shown in Figure 2. Figure 2(a) and 2(c) clearly shows that the electrons in the REM are accelerated to tens of MeV within less than 1 fs. The photon energy of the generated radiation is related to the electron energy. For the early time, the smaller electron energy will lead to radiation with a longer wavelength. As Figure 2(b) shows, the generated radiation field within the area of the REM only contains one half cycle. Then under higher electron energy, Figure 2(d) shows that several cycles are contained within the area of the REM. This temporal changing wavelength is the typical feature of the chirped pulse. Actually, the generation of the chirped attosecond pulses can also be observed in many previous simulation results (Wu *et al.*, 2010; Bulanov *et al.*, 2016).

In order to analyze the generation process of the reflected radiation, the relation between the reflected field and the corresponding generation moment can be obtained from the simulation results as shown in Figure 3(a). In Figure 3(a), there is an unusual intense peak right after the moment of 14.21 fs. This peak is generated at the second half cycle of the probe laser, where the peak laser field is four times lower than the maximum laser electric field. So, the reflectivity near this peak is obviously amplified. Then, the following emission will be terminated due to the destructive interference when the thickness of the REM becomes larger than half of the wavelength of the generated radiation.

To understand such unusual amplification, the temporal evolution for the electron energy and density of the REM can be drawn from the simulation results. The plasma frequency of the REM is

$$\omega_e = \sqrt{n_e(t)e^2/m_e\epsilon_0}, \quad (1)$$

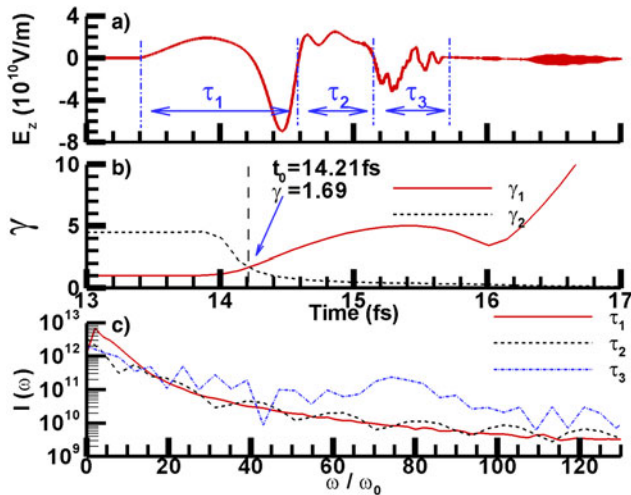


Fig. 3. (a) The relation between the radiation electric field and the corresponding generation moment. The field is divided into three sections which are indicated by the blue dash dotted lines. (b) The evolution of real energy γ_1 (red solid line) and the resonance energy γ_2 (black dashed line) of REM. (c) The spectra for the three sections are indicated by τ_1 , τ_2 , and τ_3 .

where $n_e(t)$ is the average electron density in the central part of the REM at different moment, ϵ_0 is the permittivity of free space, e is the electron charge, and m_e is the electron mass. For the REM with the energy of $\gamma_1 mc^2$, where $\gamma_1 = 1/\sqrt{1 - (v_0/c)^2}$ is the average electron normalized energy and v_0 is the electron velocity. Through the Lorentz transformation from the lab frame of reference to the REM moving frame of reference, the laser frequency ω'_L in the REM moving frame of reference can be obtained as

$$\omega'_L = \gamma_1(\omega_L - \beta \cdot k_0c) \simeq 2\gamma_1\omega_L, \tag{2}$$

where ω_L and $\beta = v_0/c$ are the laser frequency and normalized electron velocity in the lab frame of reference, respectively, and k_0 is the laser wave vector.

When ω'_L is equal to the frequency ω_e in the REM moving frame of reference, the resonance between the laser field and the plasma oscillation in the REM can lead to the amplification of reflection. Under the resonance condition, the normalized energy of REM must satisfy the relation of

$$\gamma_2(t) = \frac{\omega_e/\sqrt{\gamma_1}}{(\omega_L - \beta \cdot k_0c)} = \frac{\sqrt{n_e(t)e^2/m_e\epsilon_0/\gamma_1}}{(\omega_L - \beta \cdot k_0c)}, \tag{3}$$

which is determined by the instant density $n_e(t)$.

The evolution of γ_1 and γ_2 is shown in Figure 3(b). Initially when the electrons are static, $\gamma_1(t < 13.8 \text{ fs}) = 1$, $\omega'_L(t < 13.8 \text{ fs}) = \omega_L$, and the density $n_e(t < 13.8 \text{ fs}) = 75 n_c \gg n_c$. The probe laser is reflected without blue shift, as shown in the first half cycle in Figure 3(a). Then during the acceleration of REM, γ_1 keeps increasing and n_e keeps decreasing due to the expansion of the REM. According to Eq. (3), γ_2 will be reduced due to the increasing of γ_1 and the decreasing of n_e . The turning point is indicated by the vertically dashed black line both in Figure 3(a) and 3(b) at the moment $t_0 = 14.21 \text{ fs}$. The two lines in Figure 3(b) intersect at this point. Within a very short time interval right after this moment, the resonance condition between the laser field and the plasma oscillation in the REM is satisfied, which will lead

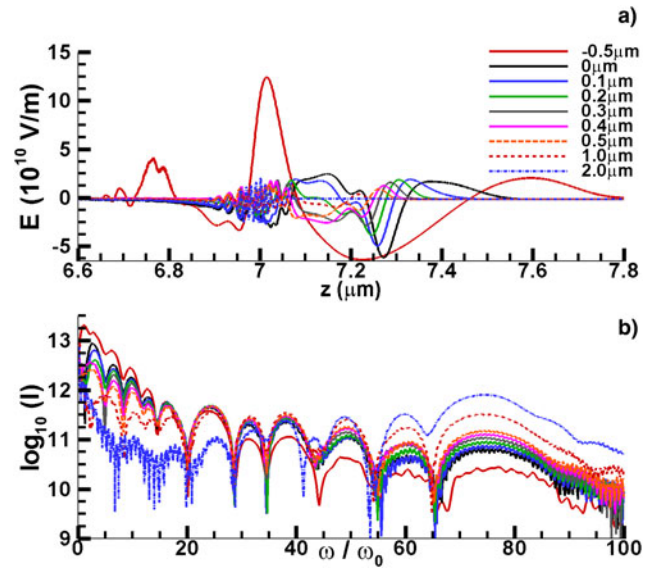


Fig. 4. (a) The reflected field for the different delay of the probe laser. The z position of the result for the delay of $-0.5 \mu\text{m}$ is slightly shifted in order to be shown with other results in the same frame. (b) The spectra of the reflected field for the different delay of the probe laser.

to the following amplification of reflection. Then with the continuous acceleration and expansion of the REM, γ_1 will be greater than γ_2 after a very short time. So the amplification due to the resonance will be terminated quickly.

In order to control and adjust the radiation spectra, it is necessary to analyze the temporal evolution of the radiation spectra. The radiation field in Figure 3(a) can be divided into three sections indicated by τ_1 , τ_2 , and τ_3 . Through Fourier analysis, the spectra for the three sections are, respectively, obtained as the three lines in Figure 3(c). For the first section indicated by τ_1 , the reflected field under the resonance condition is included. The spectrum obtained from Fourier analysis shows that this section mainly contributes to the harmonics of $\omega < 10\omega_0$. Using the formula

$$\gamma_R = \gamma_1^2(1 + \beta)^2\omega_L, \tag{4}$$

the central radiation frequency γ_R under the resonance γ of 1.69 is $9.25\omega_L$, which is consistent with the results from Fourier analysis. Then with the acceleration of the REM, the energy of the later generated photons will be higher. The section corresponding to τ_3 mainly contributes to the harmonics of $\omega > 20\omega_0$, while the contribution of the section corresponding to τ_2 is much less than those for τ_1 and τ_3 . The analyses on the temporal evolution of the radiation spectra confirm our previous conclusion that the generated radiation is a chirped attosecond pulse. Although the total duration of the chirped pulse is about 2 fs, selective frequency filtering for the spectra can be used to choose a certain part of the radiation pulse. So, attosecond pulse can be obtained from the selective frequency filtering.

Based on the results in Figure 3(b) and 3(c), one way to control and adjust the radiation spectra can be obtained. Through adjusting the origin position of the probe laser, the relative time delay between the probe laser and the REM can be adjusted. Set the results in Figures 2 and 3 corresponding to the probe laser released at delay $0 \mu\text{m}$. The origin position of the probe laser can be adjusted from -0.5 to $2.0 \mu\text{m}$. The closer release of the probe laser will make the probe laser reach the REM earlier. The corresponding field and spectra are shown in Figure 4.

When the origin position is adjusted from 0 to $-0.5\ \mu\text{m}$, the red solid line in Figure 4 shows that the lower harmonic components ($\omega < 10\omega_0$) are amplified. This amplification can be due to the higher laser field intensity at the resonance moment. Next when the REM is accelerated to higher energy, the lower laser field intensity will lead to the depression of the higher harmonic components ($\omega > 30\omega_0$). On the contrary, when the delay is changed from 0.1 to $2.0\ \mu\text{m}$, the further release of the probe laser will make the probe laser reach the REM later. The laser field intensity at the resonance moment will be lower for the further delay. So, the reflected field intensity near the resonance moment and the lower harmonic components ($\omega < 30\omega_0$) will be depressed. At this condition, the laser field intensity will be higher when the higher harmonic components ($\omega > 40\omega_0$) are generated. So the higher harmonic components will be amplified.

Summary and discussion

In conclusion, our numerical studies show that REM with ultra-high acceleration and expanding velocity can be produced from a solid nanofilm illuminated normally by an ultra-intense femto-second laser pulse with a sharp rising edge. Isolated chirped attosecond pulse can be produced through the reflection of an ultra-short probe laser on the accelerating REM.

The acceleration and expansion of the REM will make the plasma frequency of the REM equal to the frequency of the probe laser in the REM moving frame of reference within an ultra-short time interval. So, the reflected radiation near this interval could be obviously amplified due to the resonance between laser field and the plasma oscillation in the REM. The field of the reflected radiation could also be selectively amplified or depressed, through adjusting the arriving time of the probe laser. For the chirped pulse, the controlling of the field will lead to the selective adjustment of the corresponding spectra. Based on the multi-petawatt laser facility in laser Fusion Research Center (Zeng *et al.*, 2017), the corresponding REM generation and radiation experiments can be conducted in our next work.

Acknowledgments. The authors acknowledge a very helpful discussion with Dr. Chuan-Sheng Liu in U. Maryland concerning the exactly solution of electron trajectories. We are also grateful to Dr. Bai-Fei Shen in Shanghai Institute of Optics and Fine Mechanics, Dr. Wanli Shang in CAEP and Dr. Jian Zheng in USTC for the useful discussions. The authors wish to acknowledge support from the NSAF (Grant NO. U1630246), the Presidential Foundation of China Academy of Engineering Physics (Grant NO. 2014-1-017), the Science Challenge Program (Project NO. TZ2017005), the National Key R&D Program (Grant NO. 2016YFA0401100).

References

- Attwood D (1999) *Soft X-rays and Extreme Ultraviolet Radiation: Principles and Applications*. Cambridge: Cambridge University Press.
- Bulanov SV, Esirkepov TZh and Tajima T (2003) Light intensification towards the Schwinger limit. *Physical Review Letters* **91**, 085001.
- Bulanov SV, Esirkepov TZh, Kando M, Pirozhkov AS and Rosanov NN (2013) Relativistic mirrors in plasmas. Novel results and perspectives. *Physics-Uspekhi* **56**, 429.
- Bulanov SV, Esirkepov TZh, Kando M and Koga J (2016) Relativistic mirrors in laser plasmas (analytical methods). *Plasma Sources Science & Technology* **25**, 053001.
- Esirkepov TZh, Bulanov SV, Zhidkov AG, Pirozhkov AS and Kando M (2009) High-power laser-driven source of ultra-short X-ray and gamma-ray pulses. *The European Physical Journal D* **55**, 457.
- Habs D, Hegelich BM, Schreiber J, Gross M, Henig A, Kiefer D and Jung D (2008) Dense laser-driven electron sheets as relativistic mirrors for coherent production of brilliant X-ray and γ -ray beams. *Applied Physics. B, Lasers and Optics* **93**, 349.
- Kiefer D, Henig A, Jung D, Gautier DC, Flippo KA, Gaillard SA, Letzring S, Johnson RP, Shah RC, Shimada T, Fernández JC, Liechtenstein VKh., Schreiber J, Hegelich BM and Habs D (2009) First observation of quasi-monoenergetic electron bunches driven out of ultra-thin diamond-like carbon (DLC) foils. *The European Physical Journal D* **55**, 427–432.
- Kiefer D, Yeung M, Dzelzainis T, Foster PS, Rykovanov SG, Lewis CLS, Marjoribanks RS, Ruhl H, Habs D, Schreiber J, Zepf M and Dromey B (2013) Relativistic electron mirrors from nanoscale foils for coherent frequency upshift to the extreme ultraviolet. *Nature Communications* **4**, 1763.
- Kulagin VV, Cherepenin VA, Hur MS and Suk H (2007) Theoretical investigation of controlled generation of a dense attosecond relativistic electron bunch from the interaction of an ultrashort laser pulse with a nanofilm. *Physical Review Letters* **99**, 124801.
- Meyer-ter-Vehn J and Wu H-C (2009) Coherent Thomson backscattering from laser-driven relativistic ultra-thin electron layers. *The European Physical Journal D* **55**, 433–441.
- Nieter C and Cary JR (2004) VORPAL: a versatile plasma simulation code. *Journal of Computational Physics* **196**, 448–473.
- Sprangle P and Esarey E (1992) Interaction of ultrahigh laser fields with beams and plasmas. *Physics of Fluids B* **4**, 2241–2248.
- Sprangle P, Ting A, Esarey E and Fisher A (1992) Tunable, short pulse hard X-rays from a compact laser synchrotron source. *Journal of Applied Physics* **72**, 5032–5038.
- Tan F, Wu B, Zhu B, Han D, Zhao ZQ, Hong W, Cao LF and Gu YQ (2012) Numerical investigation for shape controlling of ultrathin electron layer. *Laser and Particle Beams* **30**, 489.
- Wen M, Wu HC, Meyer-ter-Vehn J and Shen B (2009) Acceleration of ultra-thin electron layer. Analytical treatment compared with 1D-PIC simulation. *The European Physical Journal D* **55**, 451.
- Wen W, Jin LL, Lu YR, Chen JE and Yan XQ (2012) Frequency tunable X-ray/ γ -ray source via Thomson backscattering on flying mirror from laser foil interaction. *Applied Physics Letters* **101**, 021102.
- Wu HC (2011) Phase-independent generation of relativistic electron sheets. *Applied Physics Letters* **99**, 021503.
- Wu H-C and Meyer-ter-Vehn J (2009) The reflectivity of relativistic ultra-thin electron layers. *The European Physical Journal D* **55**, 443–449.
- Wu H-C, Meyer-ter-Vehn J, Fernández J and Hegelich BM (2010) Uniform laser-driven relativistic electron layer for coherent Thomson scattering. *Physical Review Letters* **104**, 234801.
- Wu HC, Meyer-ter-Vehn J, Hegelich BM and Fernández JC (2011) Nonlinear coherent Thomson scattering from relativistic electron sheets as a means to produce isolated ultrabright attosecond X-ray pulses. *Physical Review Special Topics – Accelerators and Beams* **14**, 070702.
- Zeng XM, Zhou KN, Zuo YL, Zhu QH, Su JQ, Wang X, Wang XD, Huang XJ, Jiang XJ, Jiang DB, Guo Y, Xie N, Zhou S, Wu ZH, Mu J, Peng H and Jing F (2017) Multi-petawatt laser facility fully based on optical parametric chirped-pulse amplification. *Optics Letters* **42**, 2014.